Light-Scattering Studies of a Block Poly(oxyethylene–oxypropylene–oxyethylene) Copolymer in Water/o-Xylene Mixtures

Guangwei Wu and Benjamin Chu*

Chemistry Department, State University of New York at Stony Brook, Long Island, New York 11794-3400

Received October 18, 1993; Revised Manuscript Received December 17, 1993•

ABSTRACT: Laser light scattering was used to investigate the micellization, the supramolecular formation, and the pregelation process of a PEO–PPO–PEO copolymer (Pluronic L64) in water/o-xylene mixtures over the temperature range 21–45 °C. Large aggregates could coexist with small micelles and unimers at high concentrations. It was found that the micellar size remained essentially the same from dilute to concentrated solutions. However, differing from PEO-PPO-PEO copolymers in pure water, the secondary large aggregates were formed by micelle association, not close-packing. The copolymer concentration and the amount of solubilized water determined both the number and the size of the secondary large aggregates. While the effect of temperature on the micelles was much smaller than that on the large aggregates, the amount and the size of the large aggregates decreased with increasing temperature. An open-association mechanism is proposed for the equilibrium between the micelles and the secondary large aggregates.

Introduction

PEO–PPO triblock copolymers (ABA or BAB) are widely used in pharmaceutical and cosmetic industries because of their very low toxicity.[1-3] The copolymer properties can be adjusted to fit different applications by changing the total molecular weight and the length ratio of relevant blocks. Fundamental research on such triblock copolymers has attracted considerable attention.[4-22] The colloidal properties of PEO-PPO-PEO copolymers in dilute aqueous solution are relatively well understood. In most cases, the block copolymers could form uniform spherical micelles in solution over proper concentration and temperature ranges. The size of the micelles and the value of the critical micelle concentration (cmc) or critical micelle temperature (cmt) could be related to the copolymer molecular weight and composition. Gelation could occur with increasing concentration or temperature. The minimum concentration required to form a gel was determined by the total molecular weight, the PEO content of the copolymer,[2,4] and the temperature.[18,22] Generally speaking, an increase in the total molecular weight or the PEO content should decrease the minimum gelation concentration.[4] Such effects could be utilized in controlled drug delivery; for example, PEO-PPO-PEO[3] and similar copolymers (such as PEO-PBO-PEO[20] with PBO denoting poly(oxybutylene)) have been proposed as possible components in the formulation. Therefore, it is important to understand the gelation mechanism and the gel structure formed by the PEO–PPO-type triblocks. Although the report[2] on gelation by PEO–PPO copolymers could go back as early as the 1960s, the gel structure and the gelation mechanism are still obscure.

Most of the samples used in reported studies were obtained from commercial sources (e.g., BASF Co.). The composition homogeneity of the sample has not been well defined. A distribution on the PPO content could be present based on the synthesis procedure used.[18] For example, a small amount of impurity in terms of higher PPO content in the copolymer could be responsible for the anomalous behavior observed in recent studies on the supramolecular formation of the large aggregates *before* reaching the critical micelle temperature.[8,9] The behavior of the PEO-PPO-PEO copolymers in nonaqueous solvents (e.g., xylene)[5,7] differed appreciably from that in water. For example, Pluronic L64 cannot form micelles in xylene in the absence of water at room temperature.

Xylene is a relatively good solvent for PPO. The copolymer with a higher PPO content should have better solubility. Therefore, the effect of composition inhomogeneity in L64 on the supramolecular formation could be less important when compared with that in aqueous solution. In the presence of water, L64 in xylene could also form micelles and gel at higher concentrations (e.g., >50% w/v). Small-angle X-ray scattering (SAXS) could be used to study the structure of PEO-PPO-PEO copolymers in organic solvents because of the electron density difference between the solvent and the copolymers. The present work is to explore the pregelation behavior by examining the dynamics and the structure of concentrated solutions of L64 in water/xylene mixtures.

Experimental Methods

Materials and Solution Preparation. Pluronic L64 was obtained as a gift from BASF and used without further purification. The nominal molar mass of this copolymer (EO_{13}-$PO_{30}EO_{13}$) is 2.9×10^3 g mol^{-1}. Our measured weight-average and number-average molar masses were 3.7×10^3 and 3.4×10^3 g mol^{-1}, respectively.[5] HPLC-grade o-xylene was purchased from Aldrich Chemical Co. and used as recieved. The solution was prepared by first making a concentrated solution (e.g., $C \sim 0.472$ g/mL). After having stood overnight, the solution was diluted to the required concentration. The solution for light scattering was clarified by filtration through a 0.2-μm pore size Millipore filter (Millex FGS). A certain amount of clarified distilled water was added to the filtered L64/xylene solution in order to achieve the appropriate water/xylene or L64/water ratio.

Laser Light Scattering. A standard, laboratory-built spectrometer[23] was used to measure the scattered light intensity and to perform photon correlation measurements at scattering angles between 20 and 140°. An argon ion laser was used as a light source and was operated at 488 nm. The cell was held in a brass thermostat whose temperature was controlled to ±0.02 °C. A Brookhaven BI9000AT digital correlator was used to measure the intensity correlation function.

The CONTIN[24] program was used to analyze the measured intensity correlation function in order to extract information on

* Author to whom correspondence should be addressed.
• Abstract published in *Advance ACS Abstracts*, February 15, 1994.

0024-9297/94/2227-1766$04.50/0

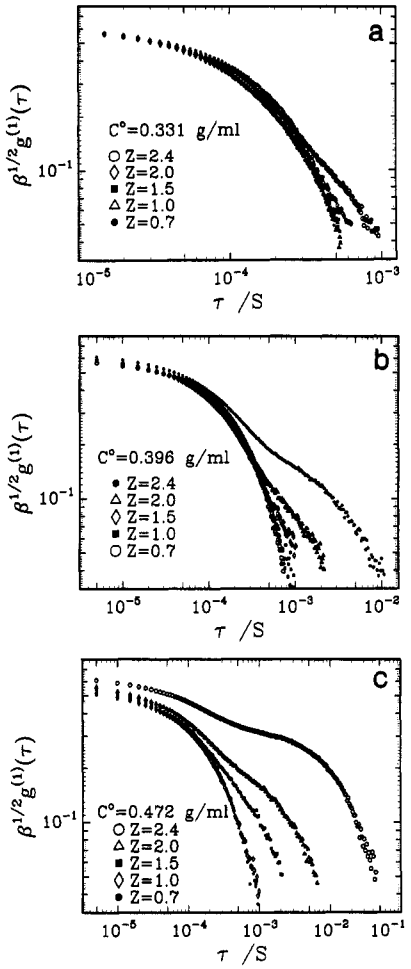

Figure 1. Plots of electric field correlation functions vs delay time(τ) at 25.0 °C and $\Theta = 90°$. Parts a, b, and c (from top to bottom) represent C° = 0.331, 0.396, and 0.472 g/mL, respectively.

the normalized characteristic relaxation rate distribution ($G(\Gamma)$). For qualitative discussion, we did not take into account of the back-flow correction at high polymer concentrations when estimating a translational diffusion coefficient (D) from the average relaxation rate ($\bar{\Gamma}$). Furthermore, the hydrodynamic radius (R_h) computed from the translational diffusion coefficient by means of the Stokes–Einstein relation is apparent since it includes the contribution based on intermolecular interactions.

Viscosity. The viscosity of the copolymer solution was measured by using a Brookfield cone–plate viscometer with a shear rate ranging from 1.15 to 230 s^{-1}. For each sample, at least three different shear rates were used. Viscosity standard solutions of 10 and 100 cP were used to calibrate the viscometer.

Results and Discussion

1. Effect of Water Amount. As we reported previously,[5,6] the micellar shape and size were determined by the water-to-EO molar ratio in micelles (Z). The maximum solubilization of L64 in xylene was about 2.7 water molecules per EO unit. With increasing Z, the micelle became larger and more asymmetric. In concentrated solutions (C(L64) > 0.30 g/mL), the solubilization ability of L64 remained almost the same. Figure 1 shows log–log plots of the electric field correlation function at three different initial L64 concentrations ($C°$ = 0.331, 0.396, and 0.472 g/mL) and five water-to-EO ratios (Z = 0.7, 1.0, 1.5, 2.0, and 2.4). The cmc was assumed to remain unchanged when we calculated the water-to-EO ratios, even though this assumption could break down at such high concentrations. The selected concentrations were far away from the cmc value (e.g., cmc = 0.086 g/mL at

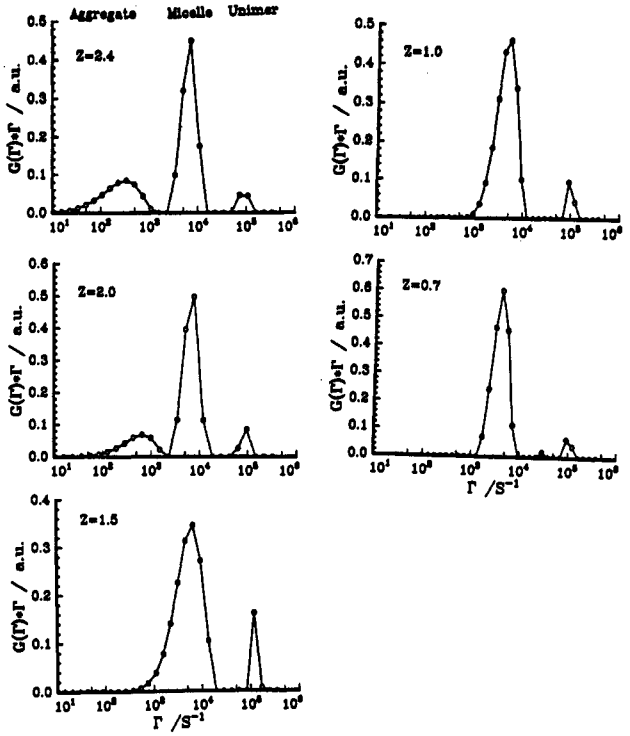

Figure 2. Relaxation rate distributions at indicated water-to-EO molar ratio in the micelle (Z) obtained by the CONTIN analysis of the field correlation functions, as shown in part b of Figure 1, at $C°$ = 0.472 g/mL.

23–24 °C as shown in ref 5), and the difference between the selected concentrations and the cmc was larger than the difference among the selected concentrations. The effects caused by changing the cmc value on Z were very close among the three different concentrations. For example, for Z = 1.5, if we assumed that the cmc value changed from 0.086 to 0.12 g/mL, the Z values would change to 1.74, 1.68, and 1.65 for $C°$ = 0.331, 0.396, and 0.472 g/mL, according to eq 15 in ref 5. In other words, the change in Z caused by a change in cmc was comparable for different $C°$. Although the micellar concentration (i.e., copolymer plus solubilized water) increased slightly with increasing Z at constant $C°$, the change in the micellar concentration was around 10% when Z was increased from 0.7 to 2.4. Therefore, an examination on the effect of water by using a series of samples based on the same $C°$ should be acceptable.

The contribution of the unimer on the intensity correlation function ($G^2(\tau)$) was reflected only in the very short delay times, i.e., at most in the first several points in Figure 1. Parts a–c of Figures 1 show that the correlation functions in the long delay time regime gradually deviated from the single-exponential behavior as the Z value was increased. This phenomenon became even more obvious as the micellar concentration was increased from $C°$ = 0.331 to 0.472 g/mL. In the case of Z = 2.4 and $C°$ = 0.472 g/mL, the correlation function was typically bimodal. The second longer delay time mode represented the presence of larger particles. In other words, larger particles were present at high Z values and high micellar concentrations. The relaxation rate of the slower mode or the size of the larger aggregates was related to the water-to-EO molar ratio and the micellar concentration (this point will be discussed in detail in the next section). The relaxation rate distributions corresponding to the conditions of Figure 1b ($C°$ = 0.396 g/mL) obtained by CONTIN analysis are shown in Figure 2. At low Z values (e.g., Z = 0.7, 1.0), only two peaks were observed. However, there were three peaks

at high Z values (e.g., $Z = 2.0, 2.4$). We assigned the fastest peak with a Γ of $\sim 10^5\ s^{-1}$ as due to the unimer contribution and the other two slower peaks to be due to the micelles and the large particles, respectively. By using the solvent viscosity in the Stokes–Einstein relation and the *apparent* translational diffusion coefficient deduced directly by $Dq^2 = \bar{\Gamma}$ and q being the magnitude of the momentum transfer vector, the *apparent* hydrodynamic radius was estimated to be 2.4 nm for $\bar{\Gamma} = 10^5\ s^{-1}$. The 2.4-nm value was in the same order as the unimer size of 1.4 nm obtained from dynamic light scattering of dilute solution of L64 in xylene.[5] On the basis of the $\bar{\Gamma}$ ratio of micelles to the unimer or large particles to the unimer, the sizes of the micelles and the large particles were estimated to be on the order of 10–20 and 100 nm, respectively. The estimated micellar size of 10–20 nm was in good agreement with the value deduced at low L64 concentrations.[5] On close examination, the peak position of the unimer in Γ at different Z values remained almost the same. Thus, we can confirm the fastest peak to be that of the unimers. With an increase in the Z values, the micellar peak ($\sim 10^4\ s^{-1}$) first became broader (e.g., at $Z = 1.5$ as shown in Figure 2). Then, a separate (slowest) peak appeared. In Figure 2, the peak area of the large agregates became larger and the peak position shifted to larger size scales with increasing Z values as demonstrated by the figures for $Z = 2.0$ and 2.4. The Z value at which a separate peak for the large secondary aggregates appeared could be related to the micellar concentration; i.e., the higher the micellar concentration, the lower the Z value required for the formation of the large secondary aggregates.

The amplitudes in $\Gamma G(\Gamma)$ from the CONTIN output denote intensity fractions, not weight fractions. The scattered intensity (I) can be expressed as

$$I \propto M_w C S(q,C) P(q) \tag{1}$$

where M_w and C are the weight-average molar mass and the concentration of the particles, respectively. $P(q)$ is the form factor, and $S(q,C)$ is the structure factor with $q \equiv (4\pi n/\lambda_0)\sin(\theta/2)$. The scattered intensity is not only proportional to the concentration, but it is also proportional to the molar mass of the particle. The large particles or aggregates had much higher molar masses than those of the micelles. Thus, the weight percentage of large particles was, in fact, quite small even though the peak areas of large particles and of the micelles were comparable at $Z = 2.4$ and 2.0 as shown in Figure 2. For example, if we take $M \propto R_h^3$, and the refractive index increments of the micelles and the large aggregates as well as the effect of interparticle interactions on the scattered intensity to be the same, the weight percentage of the large aggregates should be less than 1%.

Another interesting observation was that the peak area ratio of the micelles to the unimers (A_m/A_u) was only around 12–20 for all Z values. The aggregation number of the micelles was on the order of 100–200.[5] The concentrations and the differential refractive indices of the micelles were also higher than those of the unimers (i.e., $C >$ cmc and $(dn/dC)_m^2 > (dn/dC)_u^2$). It would seem that the peak area of the micelles should be *several orders larger* than that of the unimer. However, at finite concentrations, it was essential to take into account the effect of the structure factor, $S(q,C)$. Unfortunately, at high concentrations, it is difficult to calculate the value of $S(q,C)$ precisely. Therefore, only the peak area ratios were compared. To the first-order approximation, we used the hard-sphere model[25] to estimate the values of $S(q,C)$ and considered the micelles to be monodisperse with a measured weight-average molar mass. The sizes of both the micelles and the unimers are small when compared with the wavelength of visible light (488 nm), resulting in a negligible angular dependence. Or we can simply let $P(q) = 1$ and $S(q,C) = S(q=0,C)$ in eq 1. Based on these assumptions, the peak area ratio of the micelles and the unimers (A_m/A_u) can be expressed as

$$\frac{A_m}{A_u} = \frac{M_m C_m (dn/dC)_m^2}{M_u C_u (dn/dC)_u^2} S(q=0,C) \tag{2}$$

where M, C, and dn/dC are the weight-average molar mass, the concentration, and the refractive index increment, respectively. The subscripts m and u represent the micelle and the unimer, respectively. The detailed procedures to calculate the value of $S(q=0,C)$ have been reported in ref 5. Both the calculated values and the results from the CONTIN analysis are listed in Table I. Considering the assumptions and the uncertainties in the CONTIN analysis, the agreement between the calculated and the measured peak area ratios, which are of the same order of magnitude, is reasonable.

Table 1. Comparison of the Order of Magnitude of Theoretical Calculated and Measured Peak Area Ratio of Micelles and Unimers[a]

Z	M_n/M_u	C_m/C_u	$(dn/dC)_m^2/(dn/dc)_u^2$	$S(q=0,C)$	$(A_m/A_u)_{cal}$	$(A_m/A_u)_{mea}$
2.4	270	4.3	3.1	0.0037	13	12
2.0	225	4.2	2.7	0.0037	9.4	12
1.5	181	4.1	2.3	0.0060	10	13
1.0	151	3.9	1.9	0.0093	10	16
0.7	136	3.8	1.7	0.010	9.0	(20)

[a] $C^0 = 0.396$ g/mL. $S(q=0,C)$ was calculated by using $S(q=0,C) \approx (1-\varphi)^4/(1+2\varphi)^2$ with φ being the equivalent hard-sphere volume fraction of the micelles. A 1% change in φ could produce a 5% change in $S(q,C)$. The qualitative values of A_m/A_u came from the CONTIN where the uncertainties at $Z = 0.7$ and 1.0 are much larger than those at $Z = 2.4$ and 2.0 (see Figure 2).

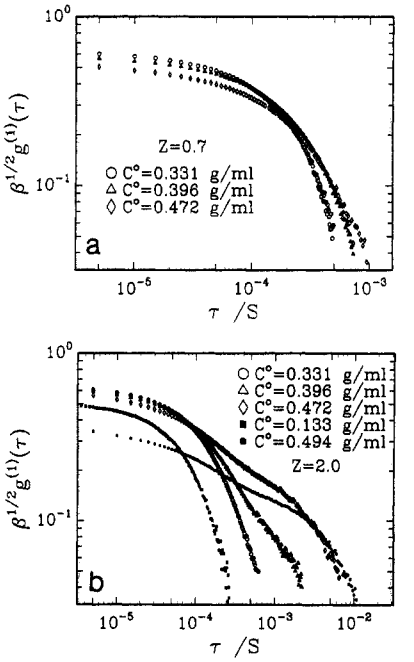

Figure 3. Plots of field correlation functions vs τ at different L64 concentrations. The correlation functions were measured at 25.0 °C and $\Theta = 90°$. Parts a and b represent the water-to-EO molar ratio in the micelle, $Z = 0.7$ and 2.0, respectively.

2. Effect of Micellar Concentration. Figure 3 shows the correlation functions at different micellar concentra-

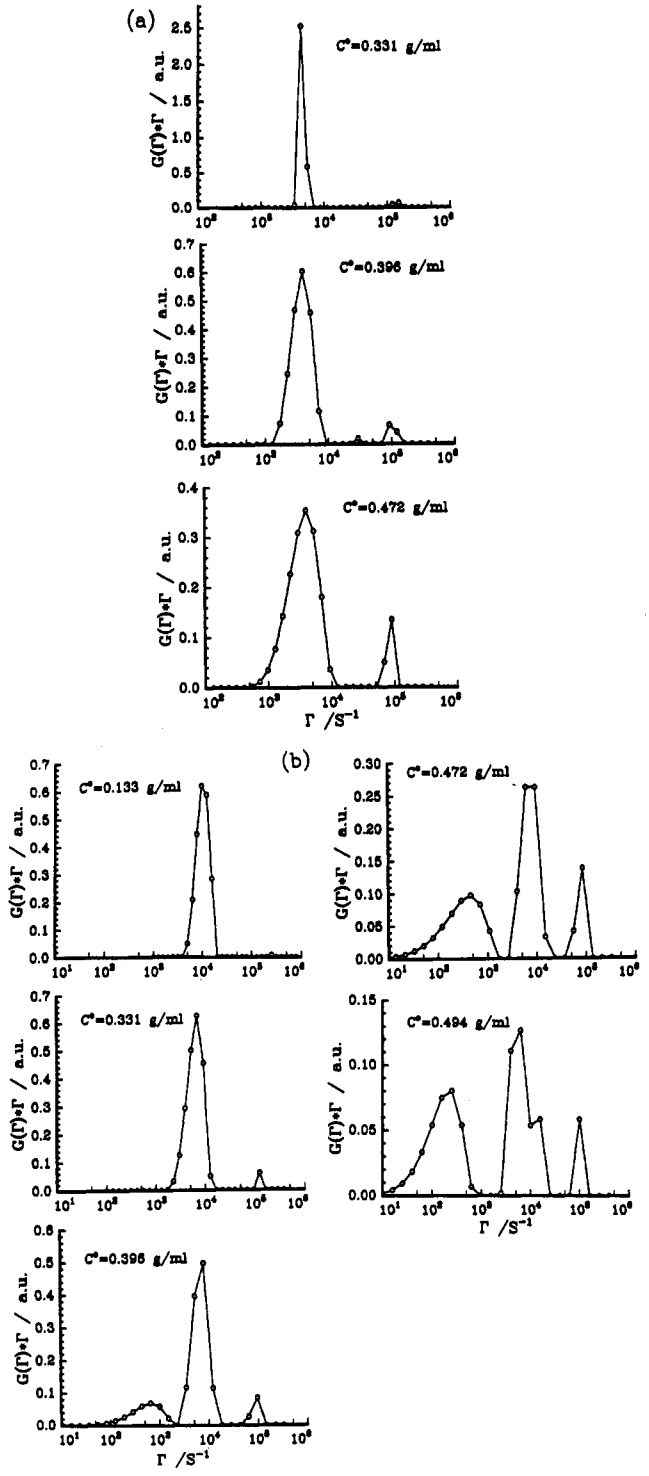

Figure 4. Relaxation rate distributions at indicated L64 concentrations obtained by the CONTIN analysis of the field correlation functions as shown in Figure 3.

tions having the same Z values: $Z = 0.7$ (Figure 3a) and 2.0 (Figure 3b). The correlation functions were similar to each other at $Z = 0.7$ and differed in the long delay time region at $Z = 2.0$. Figure 4 shows the corresponding relaxation rate distributions obtained by using the CONTIN analysis. In Figure 4b, the result at $C° = 0.133$ g/mL where only unimers and micelles existed was used as a reference. The CONTIN results did show two peaks, one for the micelles at $\Gamma \sim 10^4$ s^{-1} and the other for unimers at $\Gamma \sim 2.5 \times 10^5$ s^{-1} at $C° = 0.133$ g/mL. The peak area ratio of micelles to unimers at $C° = 0.133$ g/mL was too large to show the small peak clearly in Figure 4b. The peak area ratio from the CONTIN analysis was on the order of 1×10^2, while the estimated peak area ratio by

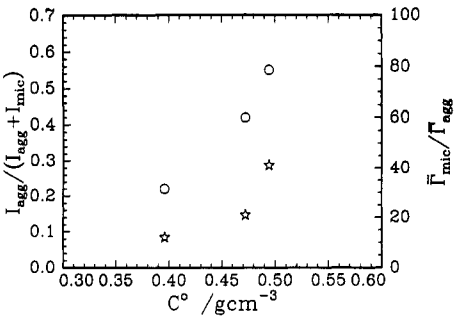

Figure 5. Intensity fraction of large aggregates, $I_{agg}/(I_{agg} + I_{mic})$, and ratio of $\bar{\Gamma}_{mic}/\bar{\Gamma}_{agg}$, as a function of initial copolymer concentration ($C°$). Both the intensity fractions (open circles) and the $\bar{\Gamma}$ ratios (open stars) were from the CONTIN analysis under the same conditions as in Figure 4b. Subscripts agg and mic denote large aggregates and micelles, respectively.

using the procedure described above was $A_m/A_u \sim 2 \times 10^2$ with $M_m/M_u \sim 230$, $C_m/C_u \sim 0.7$, $(dn/dC)_m^2/(dn/dC)_u^2 \sim 2.7$, and $S(q,C) \sim 0.4$. At low water content (e.g., $Z = 0.7$), the only difference for the micellar part was that the micellar peak became broader with increasing micellar concentration. At higher water content (e.g., $Z = 2.0$), the large particle (slowest) peak appeared when the micellar concentration exceeded a certain value. The minimum micellar concentration at which the large particle peak started to appear was determined by the Z values. This minimum micellar concentration decreased with increasing Z value. For example, the large particle peak was not observed for $Z = 0.7$. At $Z = 2.0$, a separate large particle peak was observed when $C° \geq 0.4$ g/mL. The large particle peak was present for all three concentrations ($C° = 0.331$, 0.396, and 0.472 g/mL) when $Z = 2.4$. With increases in the micellar concentration, the large particle peak position shifted slightly to larger size, became broader, and increased in amplitude, as shown in Figures 4a,b and 5. Figure 5 shows how the intensity fraction of the large aggregates, denoted by $I_{agg}/(I_{agg} + I_{mic})$, based on the CONTIN analysis varies with the micellar concentration expressed in term of the initial L64 concentration ($C°$). With the unimer contribution being very small (<10%) and remaining relatively constant, the intensity fraction of the large aggregates increased rapidly with increasing copolymer concentration. The ratio $\bar{\Gamma}_{mic}/\bar{\Gamma}_{agg}$, denoted by hollow stars, also became larger at higher concentrations, as shown in Figure 5. The size of the large aggregates was on the order of 10^2 nm, as discussed in section 1. It should be noted that the intensity fraction as we determined at finite θ depends upon the particle scattering factor ($P(q)$) since the aggregates are quite large. Therefore, the $I_{agg}/(I_{agg} + I_{mic})$ values expressed in Figure 5 should change with q. Nevertheless, the trend should remain the same. The results from another scattering angle, e.g., $\theta = 60°$, confirmed this supposition.

There are several ways for micelles to change size and/or shape when the micellar concentration is increased further. Figure 6 shows a *schematic* diagram for three *possible* scenarios induced by increasing the micellar concentration. The solid circles denote equivalent hard spheres. One observation was that at constant temperature, the micellar size and shape remained essentially unchanged and only the number of micelles increased with increasing polymer concentration. Eventually, large aggregates or certain secondary structures were formed. After the micellar concentration reached a certain value, the solution became a gel due to the close-packing of the micelles. Figure 6a shows a schematic representation of such large aggregates. The minimum micellar concen-

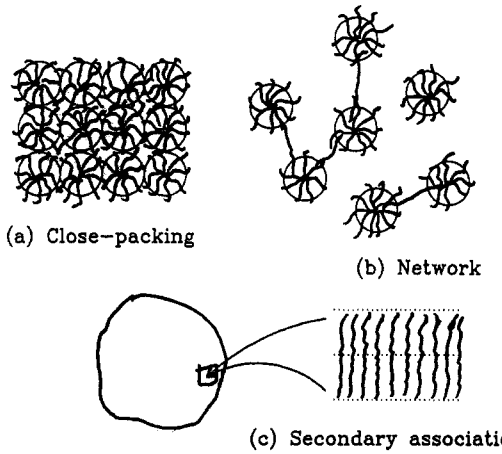

Figure 6. Schematic diagram of three possible structure formed at high micellar concentrations. Circles represent the equivalent hard-sphere size size of the micelles. The real shape of the large aggregates in c has not yet been determined.

tration required to form a gel is dependent upon the packing structure. For example, the minimum volume fractions to form a cubic, a body-centered cubic, and a face-centered cubic close-packing are 0.52, 0.68, and 0.74, respectively. A gel should form when the micelles (or the equivalent hard spheres) begin to overlap. For copolymer micelles, usually the micellar shell is heavily solvated.[26] Therefore, the gel formation could be observed at relatively lower copolymer concentrations; e.g., the Pluronic F127 water solution, the minimum gelation concentration was ~20% w/v.[4,17,18] As the micellar size distribution for our system was fairly narrow,[5] a deviation from the volume fraction for close-packing caused by polydispersity should also be small.

Another possible way could be network formation of micelles[29] bridged by chains of unimers, as depicted schematically in Figure 6b. Then, the gelation concentration should be much lower than that in the case of close-packing.

A third possible way is that the micelles will aggregate to form larger particles after the micellar concentration has exceeded a certain value. The larger secondary particles (or aggregates) could have more compact structures than the close-packing of micelles mentioned in the previous paragraph. For example, lamellar structures, as shown schematically in Figure 6c, could be formed. The large aggregates had a broad size distribution, implying that the micelles and the large aggregates were governed by an open-association equilibrium behavior. The size and the amount of the large aggregates could increase with increasing micellar concentration, as demonstrated in Figure 4b.

Large aggregates were observed in PEO-PPO-PEO/water solutions.[11] A cubic structure was proposed to describe the gel structure formed at high concentrations.[14-16] The gelation concentration of the copolymer was low, and the corresponding volume fraction of the micelles was in agreement with the minimum close-packing values.[20] However, the behavior of the PEO-PPO-PEO copolymer in xylene in the presence of water was a little bit different from that of the PEO-PPO-PEO/water solutions. All samples remained as viscous fluids, not as gels, even at micellar concentrations as high as 54% w/v. The gel was observed at higher micellar concentrations, e.g., at a concentration of >62%.[27] With the assumption that the micellar size and shape remained almost unchanged and based on the micellar parameters determined at low concentrations, it is straightforward to calculate

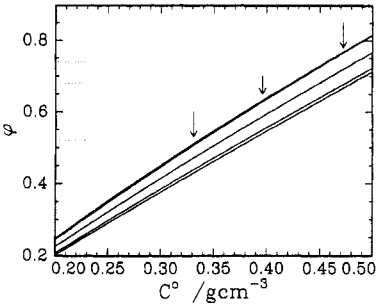

Figure 7. Relationship of equivalent hard-sphere volume fraction of micelle (φ) with initial L64 concentration ($C°$). From below to above, the water-to-EO molar ratio in the micelle is 0.7, 1.0, 1.5, 2.0, and 2.4, respectively. The three arrows denote the three concentrations used in this study, and the three dash lines represent the minimum close-packing volume fraction for the cubic, the body-centered cubic, and the face-centered cubic arrangements, respectively.

the hard-sphere volume fraction (φ_{HS}) at different copolymer concentrations and water-to-EO ratios by using the relation

$$\varphi_{HS} = \frac{C}{M_m} N_A \frac{4}{3}\pi R_{HS}^3 \qquad (3)$$

where C, N_A, and R_{HS} are the micellar concentration, Avogardro's constant, and the equivalent hard-sphere radius, respectively. The calculated φ_{HS} at different initial L64 concentrations ($C°$) and different water-to-EO ratios is shown in Figure 7. The micellar volume fraction increased with increasing L64 concentration and water-to-EO ratio. At $Z = 2.0$ and $C° = 0.494$ g/mL, the micellar volume fraction reached a value of about 0.81, higher than the minimum volume fraction required for a close-packing by the face-centered cubic structure. Gelation occurred at higher micellar concentrations when the equivalent hard-sphere volume fraction was close to 1.[27] It *seems* that in contrast to the PEO-PPO-PEO/water solutions, the larger particles formed by L64 in water/xylene mixtures might not be the result of close-packing of micelles. Therefore, we propose that the micelles first aggregate into a broad distribution of large aggregates which were governed by an open-association equilibrium. SAXS results[27] also showed that the larger particles had a lamellar structure, further supporting the proposed model.

3. Angular Dependence. Dynamic light-scattering measurements were carried out at $\theta = 45, 60, 90$, and 120°. Two typical sets of CONTIN-output results at the four different scattering angles are shown in Figure 8. Figure 8a represents the case where only the micelles and the unimers are present at $Z = 0.7$ and $C° = 0.331$ g/mL. Figure 8b shows the angular dependence on the characteristic line width at $Z = 2.0$ and $C° = 0.472$ g/mL. In both cases, the angular dependence could be normalized by q^2, implying the translational diffusive characteristic even in the presence of large aggregates.

4. Temperature Effects. Temperature plays a very important role in the micellization or the gelation of PEO-PPO-PEO copolymers in water. In order to probe the temperature effects on micelles and large particles, the intensity correlation functions were measured at six different temperatures ranging from 21 to 45 °C. The temperature effect was not obvious to those containing only micelles and unimers. The colloidal behavior was temperature dependent in the presence of large aggregates. Figure 9 shows the temperature effect on the intensity correlation functions for the cases where the intensity contributions due to the large particles were small (Figure

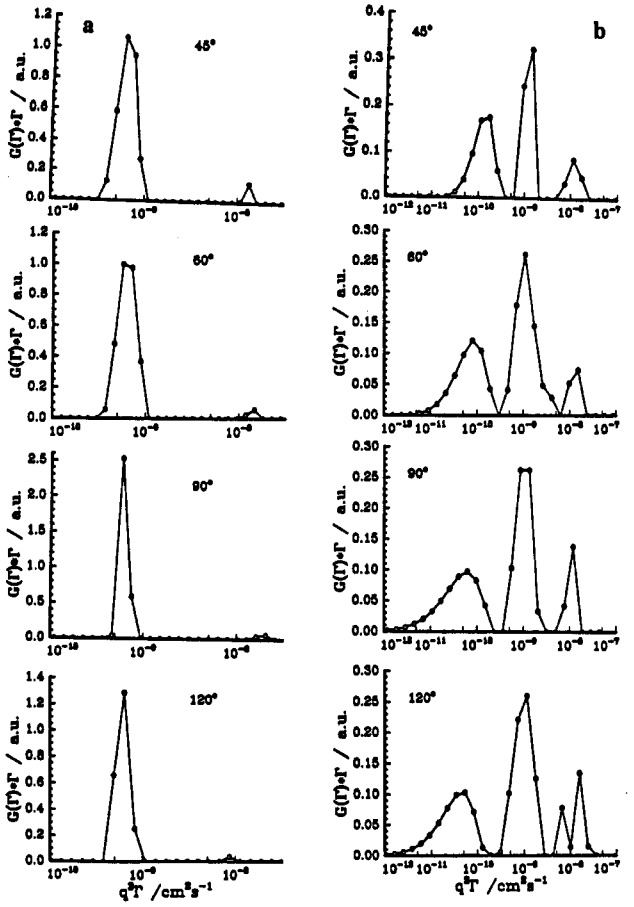

Figure 8. Relaxation rate distributions at indicated scattering angles obtained by the CONTIN analysis of the field correlation functions. Initial L64 concentrations are 0.331 and 0.472 g/mL and water-to-EO molar ratios are 0.7 and 2.0 in parts a and b, respectively.

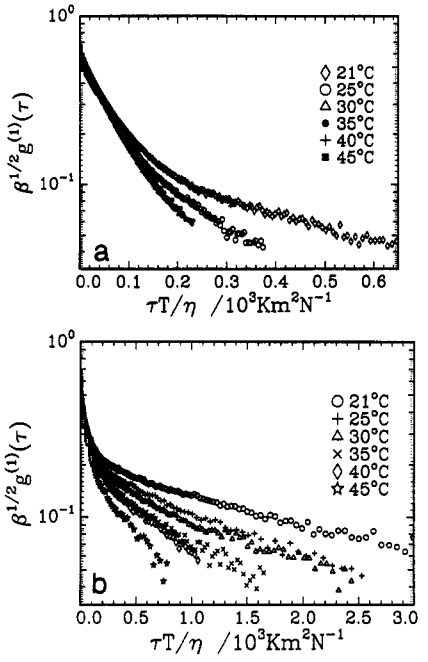

Figure 9. Plots of field correlation functions vs τ at indicated temperatures and $\Theta = 90°$. Initial L64 concentrations are 0.331 and 0.472 g/mL, and water-to-EO molar ratios in the micelle are 2.0 and 2.4 in parts a (top) and b (bottom), respectively.

8a) or comparable (Figure 8b) with the micelles. In Figure 9a, the correlation functions were affected only at low temperatures, e.g., <30 °C. At temperatures higher than 30 °C, the correlation functions were very similar to each other. The temperature effect on the correlation functions

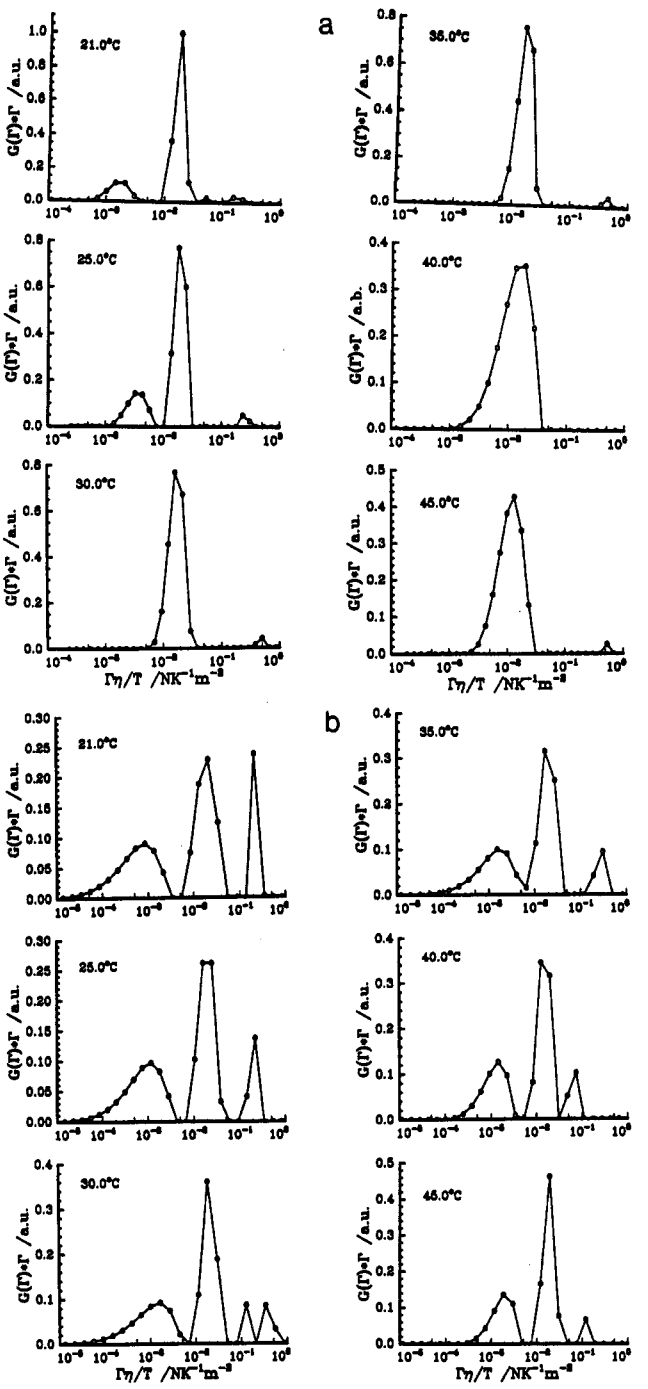

Figure 10. Relaxation rate distributions at indicated temperatures obtained by the CONTIN analysis of the field correlation functions which correspond to those in Figure 9. Water-to-EO molar ratios in the micelle are 2.0 and 2.4 in parts a (top) and b (bottom), respectively.

became more obvious and existed for all the temperatures, as shown in Figure 9b, when the intensity contribution of the large particles was comparable with that of the micelles. In both cases, the characteristic relaxation rate of the slow mode (at long delay times) became faster with increasing temperature. Figure 10 shows the corresponding relaxation rate distribution results of Figure 9, respectively. In the presence of a small percentage contribution from large particles (Figure 10a), the slow mode (related to the large particle) was shifted first to shorter time scales and then merged into the micellar mode. In other words, the large particles were "melted" away as the temperature was increased. In the presence of more large particles (Figure 10b), the slow mode was also shifted to shorter delay times and the amount was decreased. As we have discussed previously, the equilibrium between the micelles and the

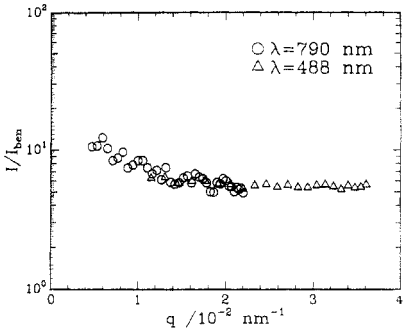

Figure 11. Scattered intensity as a function of scattering vector, q. Two symbols represent two sets of data measured by two different light-scattering spectrometers with different incident light wavelengths (λ_0 = 488 and 790 nm, respectively). The initial L64 concentration (C°) and the water-to-EO ratio (Z) are 0.473 g/mL and 1.5, respectively. One of the curves has been shifted by a constant.

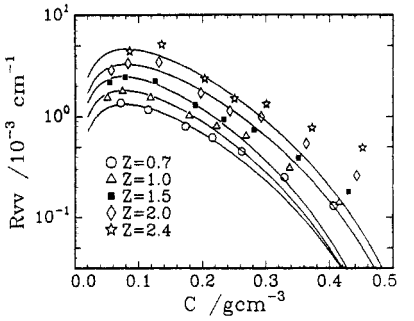

Figure 12. Relationship of excess scattered intensity (R_{vv}) with micellar concentration at indicated water-to-EO molar ratios and 25 °C. The lines are best fits of the hard-sphere model in the lower concentration range (C < 0.28 g/mL).

large particles could be considered as an open-association equilibrium. The solubility of PEO-PPO-PEO copolymers in xylene was increased with increasing temperature. Therefore, the equilibrium constant between the micelles and the large particles should decrease with increasing temperature. In other words, micelles should become more favorable with increasing temperature. The shift of large particles to smaller ones with a corresponding decrease in the amount at higher temperatures supports the proposed open-association model for equilibrium between micelles and large particles.

5. Static Light Scattering. The scattered intensity was also measured as a function of scattering angle from θ = 20 to 140°. There was no angular dependence for most samples except for a few which had a slight upturn below θ ≈ 40°, as shown in Figure 11. This slight upturn could possibly be attributed to the presence of the large aggregates. In order to reach a smaller q range, another laser-light-scattering instrument[28] equipped with a longer wavelength light source (λ_0 = 790 nm) was used to measure the angular distribution of scattered intensity. The results are shown in Figure 11. Without considering the effects of the structure factor, the magnitude of the radius of gyration (R_g) was estimated by using a Guinier plot. R_g was on the order of 10^2 nm, in agreement with the R_h value of 10^2 nm computed from the CONTIN analysis. By extrapolating the scattered intensity at high scattering angles (θ > 40°), an apparent Rayleigh ratio, R_{vv}, could be obtained. This R_{vv} could include the intensity contribution from the micelles in addition to the low limit of the intensity contribution from the large aggregates. Figure 12 shows a relationship between the apparent R_{vv} and the micellar concentration. The lines represent the best fit of the hard-sphere model for the low concentration part (C < 0.28 g/mL). The deviation of the measured values from the theoretical curve became larger with increasing concentration or Z. The deviation could be attributed to the presence of the large aggregates. At low concentrations and in the absence of the large aggregates, the R_{vv} vs C results agreed with the hard-sphere model. The observed deviations at higher micellar concentration and Z values were proportional to the amount of the large aggregates formed. On the basis of the intensity fraction of the large aggregates obtained by the CONTIN analysis at θ = 90°, the contribution of the large aggregates to the apparent R_{vv} could be estimated. After subtracting the contribution of the large aggregates, the difference between the measured R_{vv} due to the micelles and the calculated value based on the hard-sphere model became much smaller. For examples, at Z = 2.0, the calculated values of R_{vv}/C were 25, 7.8, and 1.5 10^{-4} cm^2/g at C° = 0.331, 0.396, and 0.472 g/mL, respectively. Correspondingly, the measured values before and after subtraction of contribution from the large aggregates were 34, 15, and 5.9 10^{-4} cm^2/g (before subtraction) and 31, 12, and 3.4 10^{-4} cm^2/g (after subtraction), respectively. The differences between the measured values (after subtraction of intensity contributions by the large aggregates) and the calculated R_{vv}/C were equivalent to 5.5%, 8.0%, and 8.6% changes in the volume fraction of the micelles for C° = 0.331, 0.396, and 0.472 g/mL, respectively. In other words, it is reasonable to assume that the equivalent hard-sphere approximation for the micelles remained valid even at high concentrations where the large aggregates were present. Surely, the possibility that this deviation was caused partially by the hard-sphere model cannot be excluded. Figure 13 reflects the effect of temperature on the scattered intensity. The scattered intensity increased with increasing temperature at all water-to-EO ratios. For the specific concentration, C° = 0.331 g/mL, a detectable amount of the large particles was present only at Z = 2.4. The dynamic light-scattering results showed that the micelles and the unimers were almost not affected by temperature and that the large particles became smaller with increasing temperature. A possible explanation for the increase in the scattered intensity with increasing temperature was that the interparticle interactions became weaker with increasing temperature.

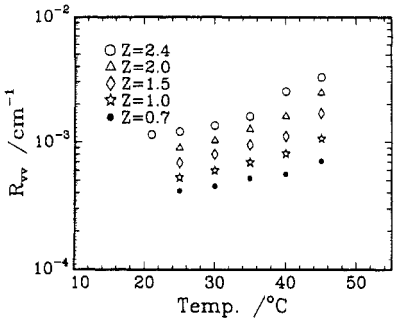

Figure 13. Excess scattered intensity at denoted water-to-EO molar ratios as a function of temperature. Initial L64 concentration (C°) is 0.331 g/mL.

6. Viscosity Measurement. A Brookfield cone–plate viscometer was used to measure the viscosity of the solutions at 25.0 °C. Within the limited shear rate range (varying for each sample and usually covering 1 decade; the more viscous the sample, the lower the shear rate used), the shear rate dependence was not observed. Therefore, an asymmetry of the large particles or a shear-induced structure could be excluded. The viscosity results are shown in Figure 14. The viscosity increased with increasing micellar concentration or Z. The rate of increase in

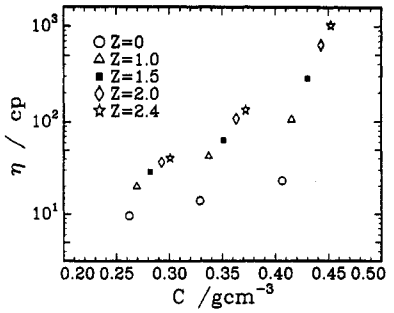

Figure 14. Viscosity of the solutions at denoted water-to-EO molar ratios as a function of micellar concentration. Viscosity was measured by using a Brookfield cone-plate viscometer at 25.0 °C.

viscosity with concentration incrased with increasing Z value. Thus, we could anticipate that the gelation concentration should decrease with increasing Z values.[27]

Conclusions

Differing from the dilute solution, large aggregates were detected by dynamic light scattering at concentrated L64 xylene/water solutions. Also differing from PEO-PPO-PEO in water, the gelation mechanism could be more like a secondary association of the micelles, not a close-packing of the micelles. The micellar size was relatively independent of temperature when compared with the temperature dependence of the large aggregates. The size of the large aggregates was on the order of 1×10^2 nm. The minimum concentration at which the large aggregates started to form could be related to the water-to-EO molar ratio (Z) inside the micelles. The minimum concentration decreased with increasing Z value. The amount and the size of the large particles increased with increasing micellar concentration or Z value and decreased with increasing temperature. An open-association equilibrium between large particles and micelles was proposed to explain the observed results. The proposed mechanism was also in agreement with the SAXS results that the larger particles had lamellar structures.[27]

Acknowledgment. We gratefully acknowledge support of this research by the U.S. Army Research Office (DAAL0391G0040) and the Polymers Program (DMR9301294), Division of Material Research, National Science Foundation.

References and Notes

(1) Schmolka, I. R. In *Polymers for Controlled Drug Delivery*; Tarcha, P. J., Ed.; CRC Press: Boston, 1992.
(2) Schmolka, I. R. *Am. Perfume Cosmet.* **1967**, *82*, 25.
(3) Chen-chow, P.-C.; Frank, S. G. *Int. J. Pharm.* **1981**, *8*, 89.
(4) Schmolka, I. R. *J. Am. Oil Chem. Soc.* **1991**, *68*, 206.
(5) Wu, G.; Zhou, Z.; Chu, B. *Macromolecules* **1993**, *26*, 2117.
(6) Wu, G.; Zhou, Z.; Chu, B. *J. Polym. Sci., Phys. Ed.* **1993**, *31*, 2035.
(7) Chu, B.; Zhou, Z.; Wu, G. *J. Non-Cryst. Solids*, accepted for publication.
(8) Zhou, Z.; Chu, B. *J. Colloid Interface Sci.* **1988**, *126*, 171.
(9) Zhou, Z.; Chu, B. *Macromolecules* **1987**, *20*, 3089; **1988**, *21*, 2548.
(10) Tontisakis, A.; Hilfiker, R.; Chu, B. *J. Colloid Interface Sci.* **1990**, *135*, 427.
(11) Schillén, K.; Brown, W.; Koňák, C. *Macromolecules* **1993**, *26*, 3611.
(12) Brown, W.; Schillén, K.; Almgren, M.; Hvidt, S.; Bahadur, P. *J. Phys. Chem.* **1991**, *95*, 1850.
(13) Brown, W.; Schillén, K.; Hvidt, S. *J. Phys. Chem.* **1992**, *96*, 6038.
(14) Mortensen, K.; Brown, W. *Macromolecules* **1993**, *26*, 4128.
(15) Mortensen, K.; Pedersen, J. S. *Macromolecules* **1993**, *26*, 805.
(16) Mortensen, K.; Brown, W. *Phys. Rev. Lett.* **1992**, *68*, 2340.
(17) Wanaka, G.; Hoffmann, H.; Ulbricht, W. *Colloid Polym. Sci.* **1990**, *268*, 101.
(18) Yu, G.-E.; Deng, Y.; Dalton, S.; Wang, Q.-G.; Attwood, A.; Price, C.; Booth, C. *J. Chem. Soc., Faraday Trans.* **1992**, *88*, 2537.
(19) Yang, L.; Bedells, A. D.; Attwood, A.; Booth, C. *J. Chem. Soc., Faraday Trans.* **1992**, *88*, 1447.
(20) Luo, Y.; Nicholas, C. V.; Attwood, D.; Collett, J. H.; Price, C.; Booth, C.; Chu, B.; Zhou, Z. *J. Chem. Soc., Faraday Trans.* **1993**, *89*, 539.
(21) Linse, P.; Malmsten, M. *Macromolecules* **1992**, *25*, 5434.
(22) Malmsten, M.; Lindman, B. *Macromolecules* **1992**, *25*, 5440.
(23) Chu, B.; Onclin, M.; Ford, J. R. *J. Phys. Chem.* **1984**, *88*, 6566.
(24) (a) Provencher, S. W. *Makromol. Chem.* **1979**, *180*, 201. (b) Provencher, S. W. *Comput. Phys. Commun.* **1982**, *27*, 213.
(25) Vrij, A.; Jansen, J. W.; Dhont, J. K. G.; Pathmamanoharan, C. *Faraday Discuss. Chem. Soc.* **1983**, *76*, 19.
(26) Tuzar, Z.; Kratochvil, P. In *Surface and Colloid Science*; Matijivic, E., Ed.; Plenum Press: New York, 1993.
(27) Chu, B.; Wu, G.; Ying, Q. *Macromolecules*, submitted for publication.
(28) Chu, B.; Ying, Q.; Dhadwal, H. S. *Rev. Sci. Instrum.* **1993**, *64*, 1659.
(29) Rodrigues, K.; Mattice, W. L. *Polym. Bull.* **1991**, *25*, 239.